

# TIME-ACCURATE TURBOMACHINERY SIMULATIONS WITH OPEN-SOURCE CFD; FLOW ANALYSIS OF A SINGLE-CHANNEL PUMP WITH OpenFOAM

Mikko Auvinen\*, Juhaveikko Ala-Juusela\*, Nicholas Pedersen†,  
Timo Siikonen\*

\*,\* Aalto University  
P.O. Box 14400 FI-00076 Aalto, Finland  
e-mail: {mikko.auvinen, juhaveikko.ala-juusela, timo.siikonen}@hut.fi  
† Grundfos A/S  
Poul Due Jensens Vej 7, DK-8850 Bjerringbro, Denmark  
e-mail: nipedersen@grundfos.com

**Key words:** CFD, OpenFOAM, Transient, Time-Accurate, Turbomachinery, Rotating Machinery, GGI

**Abstract.** *This paper presents a time-accurate analysis of a single-channel pump with a flow system characterized by highly oscillatory behavior. The analysis is performed with an open-source numerical analysis library, OpenFOAM, which features a recently implemented Generalized Grid Interface method that provides the means to conduct transient, sliding interface simulations on arbitrarily unstructured meshes. Since the complexity of the flow field demands high standards from the numerical analysis, two computational models are considered and four separate cases analyzed to investigate the solution's sensitivity to turbulence modeling, grid resolution and boundary condition treatment.*

*The report includes a detailed description of the applied CFD methodology and covers a broad range of issues that are relevant to the OpenFOAM analysis and post-processing of the simulations. The obtained time-accurate results are compared against experimental performance and LDV velocity profile measurements. The comparisons yield a wealth of information on different aspects of the analysis providing tangible guidelines and recommendations.*

*All the computational cases depicted the characteristic flow behavior of the pump distinctly, but, above all, the high-resolution grid model succeeded in capturing the nature of the flow system in striking detail.*

## 1 INTRODUCTION

Single-channel (and single-blade) pumps constitute a special family of pumps, featuring geometry designed to operate in waste water conditions without clogging. This requirement complicates the design for high hydrodynamic efficiency as the non-periodic geometry generates a complex, oscillatory flow system that is vastly dissimilar to conventional multi-blade water pumps. The demanding nature of the flow system necessitates spatially and temporally accurate computational analysis,<sup>1</sup> which utilizes a sliding interface between the rotating and stationary domains. Moreover, the requirements set by reliable design practise demand that these computationally intensive transient analyses are routinely performed with high resolution to examine potential pump prototypes in greater detail. The role of such high quality CFD in exposing the mechanisms that drive performance-deteriorating flow behavior is becoming increasingly significant.

Consequently, the drastic increase in demand for such high-fidelity CFD analyses, together with the need for more flexible, customizable tools has heightened interest in open-source and license-free software across the CFD community. In response, this study utilizes OpenFOAM,<sup>2</sup> an object-oriented numerical analysis library written in C++ with a recently implemented Generalized Grid Interface<sup>3</sup> (GGI) coupling algorithm, to conduct a comprehensive, time-accurate flow analysis of an experimental single-channel pump design.

The implementation of the GGI and the associated testing and validation work<sup>4</sup> have been brought together by the *OpenFOAM-extend project*\*, which is a collaborative undertaking that also maintains the repository hosting the OpenFOAM library package used in this study. In accordance with the mission of the *OpenFOAM-extend project*, as this study builds on the contributions of others, the work is intended to provide a user contribution to the open-source community.

This paper provides a thorough description of the performed transient analysis of an experimental single-channel pump, shown in Figure 1. The report covers the relevant computational methodologies together with the associated algorithmic fundamentals and describes the analysis of four different computational models in detail. In the end, the obtained time-accurate results are presented together with experimental performance and Laser Doppler Velocimetry (LDV) velocity profile measurements, and the effects of the different modeling choices are discussed.

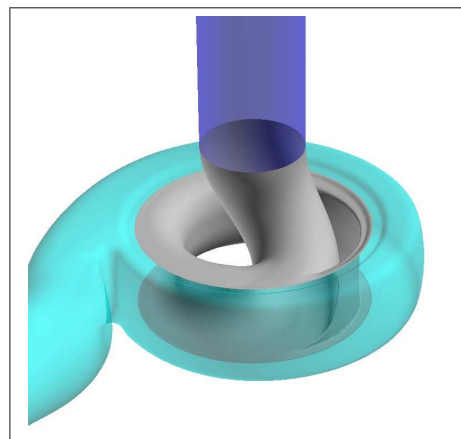


Figure 1: An overview of an experimental single-channel pump geometry.

\*<http://sourceforge.net/projects/openfoam-extend/>

## 2 CFD METHODOLOGY

The solution of the time-dependent, turbulent and incompressible flow system of the pump is governed by the Unsteady Reynolds-Averaged Navier-Stokes equations (URANS), which can be written for a moving control volume  $V$ , bounded by closed surface  $S$  with an outward pointing unit normal vector  $\mathbf{n}$ , in the following form:

$$\frac{\partial}{\partial t} \int dV + \oint (\mathbf{U} - \mathbf{U}_g) \cdot \mathbf{n} dS = 0 \quad (1)$$

$$\frac{\partial}{\partial t} \int \mathbf{U} dV + \oint \mathbf{U}(\mathbf{U} - \mathbf{U}_g) \cdot \mathbf{n} dS + \oint p \mathbf{n} dS = \oint \nu_{eff} \nabla \mathbf{U} \cdot \mathbf{n} dS \quad (2)$$

where  $\mathbf{U}$  is the fluid velocity vector and  $\mathbf{U}_g$  denotes the velocity of the bounding surface  $S$ . In Eqn.(2), the influence of the Reynolds stresses is embedded in the effective kinematic viscosity  $\nu_{eff}$ , according to Boussinesq's approximation, necessitating the use of an appropriate turbulence model to attain closure.

In a more general treatment, where the deformation of control volumes is also considered, an additional requirement must be satisfied:

$$\frac{\partial}{\partial t} \int dV + \oint (\mathbf{U}_g \cdot \mathbf{n}) dS = 0 \quad (3)$$

This is known as the *Geometric Conservation Law*.<sup>5</sup> In turbomachinery applications, where the moving grid domain undergoes only solid body rotation, this condition is evidently satisfied.

Employing the extensive library structure of OpenFOAM, two flow solver types utilizing segregated velocity-pressure coupling algorithms and featuring both automatic mesh motion and deformation functionality,<sup>6</sup> have been developed by the community for simulating the flow systems described by Eqns.(1-3). The first, entitled *pimpleDyMFoam\**, is based on the PISO<sup>7</sup> algorithm while the second, *transientSimpleDyMFoam†*, implements a time-accurate SIMPLE<sup>8</sup> pressure correction method. Although the PISO solver facilitates an accurate transient solution, it suffers from inefficient temporal time marching due to a restricting limitation on the maximum time step length. For this reason it has proven impractical for turbomachinery applications. On the other hand, the solver featuring SIMPLE does allow more aggressive time marching – naturally at the expense of temporal accuracy, which is critical in performing efficient time-accurate analysis of flow systems whose transient behavior evolves over a comparatively long time. Therefore, in this study the simulations are carried out with *transientSimpleDyMFoam*, whose principal algorithmic description is provided in the following section.

\* Available in OpenFOAM 1.6 and in OpenFOAM 1.5 as *turbDyMFoam*

† Developed under OpenFOAM-extend project (<http://openfoam-extend.sourceforge.net>) and, therefore, resides in the OpenFOAM-dev release.

## 2.1 Flow Solver

In order to provide an informative description of the *transientSimpleDyMFoam* flow solver, which implements the segregated SIMPLE pressure-velocity coupling algorithm, a proper groundwork must be laid by presenting a concise derivation of the pressure equation<sup>9</sup> as it is implemented in OpenFOAM. The grid can be considered stationary in the treatment because, within a time step, the pressure-correction step operates in an absolute velocity field.

### 2.1.1 Theoretical Background

Firstly, equations (1) and (2) are written in a discrete form for a fixed control volume  $V$  (i.e. cell) that is bounded by an arbitrary number  $N_f$  of cell faces. Given the surface area of a cell face  $S_f$ , its normal vector  $\mathbf{n}_f$  and the definition of a face flux  $\phi_f = (\mathbf{U}_f \cdot \mathbf{n}_f)S_f$ , the equations can be written as:

$$\sum_f^{N_f} (\mathbf{U}_f \cdot \mathbf{n}_f) S_f = 0, \text{ or simply: } \sum_f^{N_f} \phi_f = 0 \quad (4)$$

$$\frac{\Delta \mathbf{U}}{\Delta t} V + \sum_f^{N_f} \phi_f \mathbf{U}_f - \sum_f^{N_f} (\nu_{eff} \nabla \mathbf{U} \cdot \mathbf{n})_f S_f = - \sum_f^{N_f} p_f \mathbf{n}_f S_f \quad (5)$$

The discrete momentum equation (5) can be transformed into a linear system of equations that, for each computational cell center  $P$  surrounded by  $N_{nb}$  neighboring cells, obtains a form:

$$a_P \mathbf{U}_P + \sum_{nb}^{N_{nb}} a_{nb} \mathbf{U}_{nb} = \mathbf{RHS} \quad (6)$$

where the dimensions of the system have been changed due to a division by cell volume  $V_P$ . The right-hand-side (**RHS**) of the equation contains the source contributions arising from the discretizations of the transient, convection and diffusion terms and the pressure gradient. For convenience, the contributions are split into velocity- and pressure-dependent parts  $\mathbf{RHS} = \mathbf{rhs}(\mathbf{U}) - \nabla p$ , recognizing that  $\nabla p = (\frac{1}{V}) \sum_f p_f \mathbf{n}_f S_f$ . Using short-hand notation

$$\mathbf{H}(\mathbf{U}) = - \sum_{nb}^{N_{nb}} a_{nb} \mathbf{U}_{nb} + \mathbf{rhs}(\mathbf{U})$$

Eqn. (6) can be expressed as

$$a_P \mathbf{U}_P = \mathbf{H}(\mathbf{U}) - \nabla p \quad (7)$$

From this formulation, a new face velocity can be defined that is interpolated onto the cell faces using cell center values:

$$\mathbf{U}_P = \frac{\mathbf{H}(\mathbf{U})}{a_P} - \frac{\nabla p}{a_P} \quad (8)$$

$$\mathbf{U}_f = \left( \frac{\mathbf{H}(\mathbf{U})}{a_P} \right)_f - \left( \frac{1}{a_P} \right)_f (\nabla p)_f \quad (9)$$

The discrete pressure equation is obtained by substituting Eqn.(9) into the continuity requirement of Eqn.(4), yielding

$$\sum_f^{N_f} \left[ \left( \frac{1}{a_P} \right)_f (\nabla p)_f \right] \cdot \mathbf{n}_f S_f = \sum_f^{N_f} \left( \frac{\mathbf{H}(\mathbf{U})}{a_P} \right)_f \cdot \mathbf{n}_f S_f \quad (10)$$

A simplified form resembling the implementation in OpenFOAM can be attained by defining an intermediate velocity field and evaluating the flux field, which does not satisfy the continuity requirement, accordingly

$$\mathbf{U}^* = \left( \frac{\mathbf{H}(\mathbf{U})}{a_P} \right) \quad (11)$$

$$\phi_f^* = (\mathbf{U}_f^* \cdot \mathbf{n}_f) S_f \quad (12)$$

Thereby, the discrete pressure equation reaches its final form:

$$\sum_f^{N_f} \left[ \left( \frac{1}{a_P} \right)_f (\nabla p)_f \right] \cdot \mathbf{n}_f S_f = \sum_f^{N_f} \phi_f^* \quad (13)$$

### 2.1.2 Solver Description

Referring to the developments in Section 2.1.1 the solution procedure implemented in *transientSimpleDyMFoam* can be illustrated by the following procedure:

**TIME Loop:** while ( $t^n < t_{end}$ )

- 1) Increment time:  $t^n = t^{n-1} + \Delta t$ .
- 2) Convert face fluxes to correspond to an absolute velocity field:  
 $\phi_f = (\mathbf{U}_f \cdot \mathbf{n}_f) S_f$ .
- 3) Apply mesh movement (and/or deformation) utilizing a chosen dynamic mesh library.
- 4) Correct the flux field if the mesh has deformed. (Not necessary in turbomachinery applications.)
- 5) Convert face fluxes to correspond to a relative velocity field:  $\phi_f = (\mathbf{U} - \mathbf{U}_g)_f \cdot \mathbf{n}_f S_f$ .

6) **SIMPLE Loop:** for( i = 0; i < nIter ; i++)

6.1: Build the momentum equation (6) applying relaxation  $0 < \alpha_u < 1$  to increase the diagonal dominance of the coefficients matrix:

$$\frac{a_P}{\alpha_u} \mathbf{U}_P^i + \sum_{nb}^{N_{nb}} a_{nb} \mathbf{U}_{nb}^i = \mathbf{RHS} + \frac{(1 - \alpha_u)}{\alpha_u} a_P \mathbf{U}_P^{i-1} \quad (14)$$

and solve for  $\mathbf{U}^i$ . (Note that at the matrix level the terms are multiplied by cell volume  $V_P$  before the relaxation is applied.)

6.2: Define an intermediate velocity field  $\mathbf{U}^*$  and compute a corresponding flux field  $\phi_f^*$  according to Eqns. (11) and (12).

6.3: Store the pressure value of the current iteration:  $p^{i-1} = p^i$ .

6.4: Build the pressure equation (13) and solve for  $p^i$ .

6.5: Correct the flux field such that it fulfills the continuity requirement:

$$\phi_f = \phi_f^* - \left( \frac{1}{a_P} \right) (\nabla p^i)_f \cdot \mathbf{n}_f S_f$$

6.6: Apply an explicit relaxation to the pressure field  $p^i = p^{i-1} + \alpha_p(p^i - p^{i-1})$ , where  $\alpha_p$  is the under-relaxation factor for pressure that typically takes on values within range  $0.1 \leq \alpha_p \leq 0.3$ .

6.7: Convert face fluxes to correspond to a relative velocity field:

$$\phi_f = (\mathbf{U} - \mathbf{U}_g)_f \cdot \mathbf{n}_f S_f.$$

6.8: Correct the velocity field utilizing a relaxed pressure field according to Eqn.(8):

$$\mathbf{U}^i = \mathbf{U}^{*i} - \frac{\nabla p^i}{a_P}$$

6.9: Solve turbulence model equations.

6.10: Return to 6.1 or continue.

7) Return to 1) or exit time loop and terminate simulation.

## 2.2 Computational Models

This study focuses on simulating the main flow system of the pump, which dictates the hydrodynamic quality of the design, and, therefore, some specific aspects of the pump arrangement are neglected. For instance, the computational models do not include the water-filled cavities which emerge in the spaces separating the impeller hub and shroud from the pump housing. Consequently, the relatively small gaps which separate the rotating impeller from the stationary volute and merge the main flow path with the cavities are also omitted from the analysis. The model simplifications are well justified from a computational perspective, but inevitably hinder comparability between the numerical and experimental results.

However, in design practice the main objective is to reach comparative improvements. Thus, the principal concern lies in securing the quality of the CFD analysis such that the small changes in the hydrodynamic design are reflected in the numerical results. For this reason, strong emphasis has been placed on producing high quality grids consistently through a templatable process. These requirements have been achieved with a grid generation tool called *GridPro*.<sup>10</sup> Its technology has been thoughtfully exploited to generate hexahedral meshes for a configuration where the rotating domain is separated from the stationary by a cylindrical interface, as shown in Figure 2. The coupling across the non-conformal grid interface is handled by the GGI.

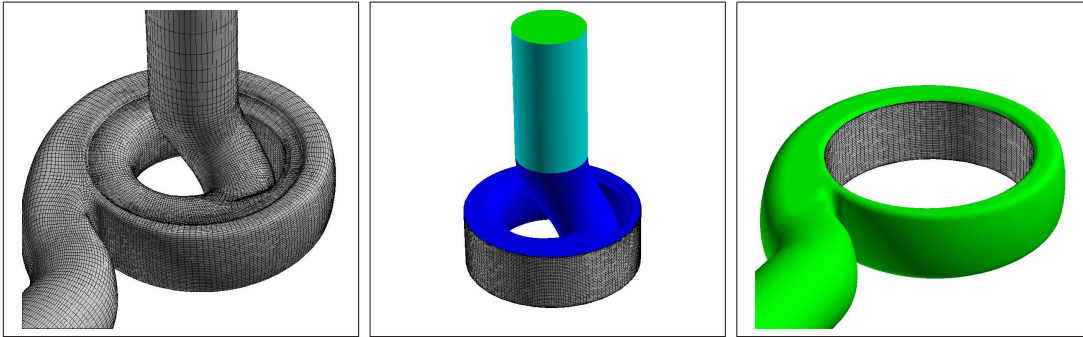


Figure 2: The CFD models consist of rotating (middle) and stationary (right) domains, which are coupled across the shown grid interface by GGI.

To investigate the effect of grid resolution, two different grid densities are considered in this study. Both grids are generated for high Reynolds number turbulence models, which employ wall functions at the solid boundaries. The grids are depicted in Figure 3 and labeled *Coarse* ( $\approx 0.5M$  cells) and *Fine* ( $\approx 1.5M$  cells), respectively. The mesh conversion to OpenFOAM format was accomplished with *GridPro2Foam*\* converter.

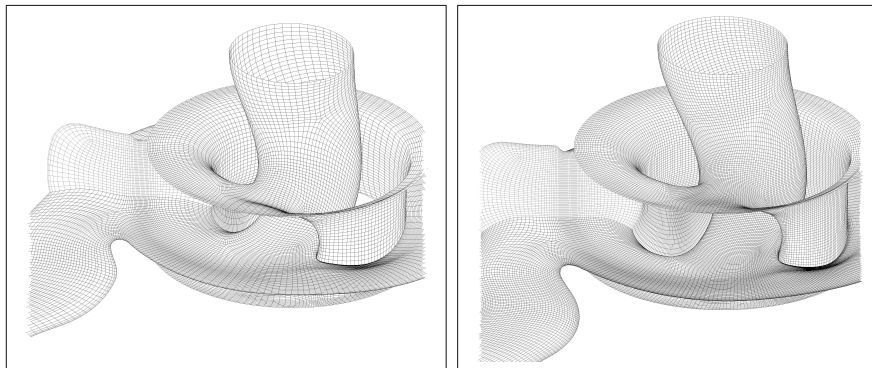


Figure 3: General view of the *Coarse* (left) and the *Fine* (right) *GridPro* grids.

\*Available at <http://www.rtech-engineering.com/news.html>

From a computational point of view, the treatment of the inflow boundary conditions turns out to be problematic: Imposing constant velocity and turbulence quantities at a location where a developed (or developing) pipe flow truly occurs clearly represents a compromising approximation. This introduces uncertainties whose level of severity should be investigated. For this purpose, a second computational model has been prepared by appending an elongated inlet duct to the **Coarse** model to allow the pipe flow profile to develop before reaching the original inflow boundary. The computational models are shown in Figure 4. The appended duct is part of the stationary domain and is also connected to the rotating domain via GGI.

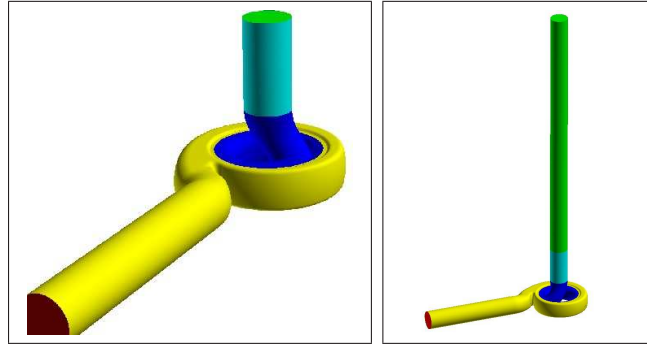


Figure 4: Outline of the standard model (left) and the elongated inlet duct model (right).

### 2.3 CFD Analysis and Case Specifications

The transient simulations are performed for the pump’s design point conditions, which were also present in the experiment performed in collaboration with the manufacturer *Grundfos*. The associated boundary conditions applied in the CFD analysis are listed in Table 1.

Solution Variable	Rotating Walls	Stationary Walls	Inlet	Outlet
$\mathbf{U}$	$\mathbf{U}_{wall} = (\boldsymbol{\Omega} \times \mathbf{r})$ $ \boldsymbol{\Omega}  = 1470 \text{ rpm}$	Fixed Value: $\mathbf{U}_{wall} = \mathbf{0}$	Fixed Value: $\mathbf{U}_{in}$ $(\rho \mathbf{U}_{in} \cdot \mathbf{n})S = 27.8 \text{ kg/s}$	Zero Gradient
$p$	Zero Gradient	Zero Gradient	Zero Gradient	Fixed Value: $p_{out}$
$k$	Wall Function	Wall Function	Fixed Value: $k_{in}$	Zero Gradient
$\varepsilon$	Wall Function	Wall Function	Fixed Value: $\varepsilon_{in}$	Zero Gradient
$\omega$	Wall Function	Wall Function	Fixed Value: $\omega_{in}$	Zero Gradient

Table 1: Applied boundary conditions.

The computational cases included in this study were constructed to yield information about numerous aspects concerning transient analysis of turbomachinery with OpenFOAM. Yet, the main elements of consideration, besides overall solution quality, were

limited to the effects of grid resolution, turbulence modeling and treatment of the inlet boundary condition. A listing of the essential computational settings characterizing the four different cases is shown in Table 2. The labeling of the numerical schemes adheres to the OpenFOAM syntax in which, for example, the suffix “V“ denotes a scheme for a vector variable, while the scalar following the name specifies the level of applied limiting. Due to their low numerical diffusion characteristics, *limitedLinear* schemes were utilized with the high resolution **Fine** grid, while the more robust *Gamma*<sup>11</sup> schemes were employed with the **Coarse** models. Despite having numerical accuracy as a high priority, the effect of the different discretization methods on the numerical results were not thoroughly investigated in this study. Experience has shown that on high quality grids most higher order discretization schemes perform well and the need for associated limiters is reduced.

<b>Grid, Turbulence Model</b>	<b>Fine, <math>k - \omega</math> SST</b>	<b>Coarse, <math>k - \omega</math> SST</b>	<b>Coarse Long, <math>k - \omega</math> SST</b>	<b>Coarse, <math>k - \varepsilon</math></b>
<b>Time-Step Size</b> $\Delta\theta =  \Omega  \Delta t$	$\Delta\theta = 0.5^\circ$	$\Delta\theta = 0.5^\circ$	$\Delta\theta = 0.5^\circ$	$\Delta\theta = 0.5^\circ$
<b>Time Derivative Schemes:</b>	backward 2 <sup>nd</sup> order	Euler 1 <sup>st</sup> order	Euler 1 <sup>st</sup> order	Euler 1 <sup>st</sup> order
<b>Convection Schemes:</b>	<b>U:</b> ILV 0.35 $k, \omega$ : IL 1.	<b>U:</b> GammaV 0.5 $k, \omega$ : Gamma 1.	<b>U:</b> GammaV 0.5 $k, \omega$ : Gamma 1.	<b>U:</b> GammaV 0.5 $k, \varepsilon$ : Gamma 1.
<b>Relaxation Factors:</b>	$\alpha_u=0.75$ $\alpha_p=0.3$ $\alpha_{k,\omega}=0.5$	$\alpha_u=0.95$ $\alpha_p=0.1$ $\alpha_{k,\omega}=0.65$	$\alpha_u=0.95$ $\alpha_p=0.1$ $\alpha_{k,\omega}=0.65$	$\alpha_u=0.95$ $\alpha_p=0.1$ $\alpha_{k,\varepsilon}=0.65$
<b>SIMPLE Loop nIter:</b>	nIter = 8	nIter = 6	nIter = 6	nIter = 6

Table 2: A case-specific listing of parameters and schemes used in the CFD analysis. Note the abbreviation: IL(V)=limitedLinear(V).

The transient simulations considered in this report were carried out exploiting techniques that aim to minimize the total CPU time required to complete the analysis. At first, using the **Coarse** model, an initial flow field was solved using a quasi-steady (or frozen-rotor) method for the purpose of providing a starting point for the time-accurate simulation. Unfortunately, due to the non-periodic geometry of the single-channel pump, the quasi-steady results misrepresent the true nature of the flow system to such degree that in the transient analysis up to nine complete revolutions were required to convect the ‘nonsense’ out of the system and reach a recurring periodic behavior. Since this lengthy evolution of the flow field was not of principal interest, it was beneficial to use a larger time step to advance the solution efficiently until higher accuracy analysis became feasible. In the build-up phase of the **Coarse** model, the time steps used corresponded up to  $\Delta\theta = 3^\circ$  and were employed together with modified solution parameters (relaxation factors, inner iterations, etc.) and discretization schemes. Once the flow field had

evolved sufficiently, the temporally and spatially accurate settings were activated and the computation was continued (at least four complete revolutions) to ensure two successive revolutions demonstrated identical performance behavior.

Substantial time was saved by taking advantage of a utility called *mapFields*, which enabled the flow solution to be copied from the **Coarse** grid to the **Fine** grid. This provided an excellent jump-start for the computationally intensive case. The same utility was used to initiate the **Coarse Long** simulation, although the mapping could not influence the added inlet duct. Nonetheless, the reduction in computational time was notable.

### 2.3.1 On Relaxation and Convergence

When solving the time-accurate Navier-Stokes equations (2), the matrix equation's diagonal dominance is principally due to the time derivative term ( $V/\Delta t$ ), which becomes insufficient for numerical stability on larger time steps. For this reason, the diagonal dominance is further increased by applying relaxation to the matrix equation, as shown in Eqn.(14), requiring that the solution must be iteratively solved until convergence within every time step. However, as is well known about iterative pressure-correction schemes, such as SIMPLE, that are mainly applied to steady-state computations, the role of relaxation is not clearly defined due to application- and numerical scheme-specific dependencies. Yet, the iterative nature of the solution method gives way to permissive standards which simplify the practical aspects considerably.

The picture is slightly more complex with URANS simulations since the role of the physical time step length and grid density are added into the mix. In this study the physical time step length was determined according to the accuracy requirement set by the hydrodynamic system of the pump, and the relaxation factors for the solution variables were set to ensure smooth numerical behavior within each time step. The variation between relaxation factors for the **Fine** and the **Coarse** models lays bare the effect of grid resolution with a given time step: The physical time step provides nearly sufficient diagonal dominance for the matrix equation on the **Coarse** grid, while significant relaxation is needed for the **Fine** case in order to ensure robust behavior. Even though the transient SIMPLE algorithm is not sensitive to any Courant number  $CFL$  criteria, it is meaningful to look at the mean Courant numbers of the two cases as they clearly reflect the underlying numerical difference.

$$\begin{aligned} \text{Fine: } CFL_{mean} &= 0.0377 \\ \text{Coarse: } CFL_{mean} &= 0.0266 \end{aligned}$$

as the Courant number in OpenFOAM is computed per cell face:

$$CFL = \frac{\phi_f \Delta t}{S_f |\Delta \mathbf{x}_{cc}|}$$

where  $|\Delta \mathbf{x}_{cc}|$  is the distance between the adjacent cell centers. The maximum Courant

numbers were practically equal for the two models because of nearly identical grid refinement close to the walls.

While smooth numerical behavior was achieved for a wide range of time steps – and mean Courant numbers – the time-accurate evolution of the pressure field began to demonstrate irregular behavior as the physical time step was reduced such that the mean Courant number reached the reported **Coarse** range. As will be seen in the pressure results in Section 3, the **Coarse** model generates small high-frequency oscillations which are visible in the hydrodynamic head graphs. These small-scale oscillations become subdued as the mean Courant number is increased, as is the case with the **Fine** model or when the time step is increased with the **Coarse** grid.

Through numerical testing it was established that, within a time step, a three orders of magnitude reduction in residuals served as a sufficient convergence criterion for the velocity and turbulence variables, while the coincident convergence of one order of magnitude (or even less) in pressure was found to be adequate. Stricter criteria did not have any detectable effects on the solutions.

## 2.4 Performance Analysis and Post-Processing

The assessment of the hydrodynamic performance of the pump is based on control volume analysis of the First Law of Thermodynamics, which, when applied to a pump with adiabatic walls and no heat source, yields the following relation:

$$\dot{W}_s = \dot{E}_T + \dot{m} (h_{T_{OUT}} - h_{T_{IN}}) \quad (15)$$

where  $\dot{W}_s$  denotes the rate of shaft work done on the system (i.e. shaft power),  $\dot{E}_T$  is the time rate of change of total energy within the system,  $\dot{m}$  is the mass flow rate through the pump and  $h_T$  stands for the total specific enthalpy. Utilizing notation  $\Delta$  to indicate differences between the values at the outlet and inlet, and the definition of total pressure for incompressible flow ( $p_T = p + 1/2\rho\mathbf{U} \cdot \mathbf{U}$ ), the energy balance can be written

$$\dot{W}_s = \dot{E}_T + \dot{m} [\Delta e + \Delta (p_T/\rho)] \quad (16)$$

as  $\Delta e$  represents the change of internal energy across the system. Recognizing that the only mechanism contributing to the change in internal energy across the system is dissipation due to viscous stresses (i.e.  $\Phi = \dot{m}\Delta e$ ) and  $\dot{W}_s = \mathbf{T} \cdot \boldsymbol{\Omega}$ , where  $\mathbf{T}$  is the torque on the impeller, Eqn. (16) can be written in a simple, but informative form:

$$\mathbf{T} \cdot \boldsymbol{\Omega} = \dot{E}_T + \Delta E_M + \Phi \quad (17)$$

where  $\Delta E_M = \dot{m}\Delta (p_T/\rho)$  is the rate of mechanical energy change across the system, or power output. The terms in the equation represent different energy budgets that allow the hydrodynamic performance of the pump to be evaluated. In pump analysis this is typically aided by two additional measures which are derived from (17), namely total hydrodynamic head,  $H$ , and efficiency,  $\eta$ :

$$H = \frac{\Delta E_M}{\dot{m}g} \quad (18)$$

$$\eta = \frac{\Delta E_M}{\mathbf{T} \cdot \boldsymbol{\Omega}} \quad (19)$$

Here it should be noted that in time-accurate simulations the role of  $\dot{E}_T$  on the right-hand-side of Eqn.(17) complicates the continuous monitoring of performance because the balance between the budgets is time dependent; the mechanisms that transfer energy from one budget to another do not operate synchronously. However, this does not affect the time-averaged measures, taken over a complete revolution, because the flow physics require that  $\dot{E}_{T_{avg}} = 0$ .

To accomplish the time-accurate monitoring of system performance in a flexible and convenient manner, OpenFOAM's built-in machinery for function objects was harnessed to develop a specific analysis tool for turbomachinery. With this function object the transient performance data could be gathered irrespective of the flow solver used for the analysis and across any set of user-defined boundary patches. The same boundary patches were used with all the models to extract the data, including the **Coarse Long** model where the GGI patch, at the interface between the added duct and the original model, functioned as a monitoring inlet.

To construct a velocity profile comparison between CFD results and LDV measurements, a utility called *sample* in the OpenFOAM library was used to extract velocity values along specified lines within the domain for every four degrees. A number of flow visualization animations were created for the same saved solution states (90 in total), which were then joined together with the velocity comparison animations to yield a highly informative depiction of the transient behavior of the system. All the data handling and plotting needed for assembling the performance results and animations were accomplished with simple *Python*\* scripts.

### 3 RESULTS AND DISCUSSION

The transient simulations conducted in this study generated a vast volume of data, which, after proper post-processing, yielded a tremendous amount of information on both the hydrodynamic performance and the behavior of the pump. While the extraction of the performance data is straight-forward and can be done on-the-fly as the computation progresses, acquiring knowledge about how the geometric features of the design affect the flow behavior requires a considerably more arduous process and demands appropriate visualization and post-processing tools. This section is arranged so that the results concerning the performance analysis are first presented and then followed by an account of the velocity profile comparisons and flow visualizations, which bring further insight to the complex flow behavior of the pump.

---

\*<http://www.python.org/>

### 3.1 Performance Comparison

The time-accurate behavior of the performance measures, shown in Figure 5, exhibit distinctly the oscillatory nature of the flow system and demonstrate the differences between the numerical modeling choices. From the hydrodynamic head and impeller force plots it becomes apparent that both **Fine** and **Coarse** grids, regardless of the chosen turbulence model, generate nearly identical pressure solutions, providing only marginally different time-averaged head values, as shown in Table 3. The small-scale pressure fluctuations, which are hardly visible in the **Fine** graphs but notable in the **Coarse** results, are solely due to numerical issues, as discussed in section 2.3.1. One should note, however, that these fluctuations show no effect on the impeller forces and very little effect on the shaft power, indicating that the fluctuations occur on a global scale and thereby have only a small influence on the solution of the momentum equation.

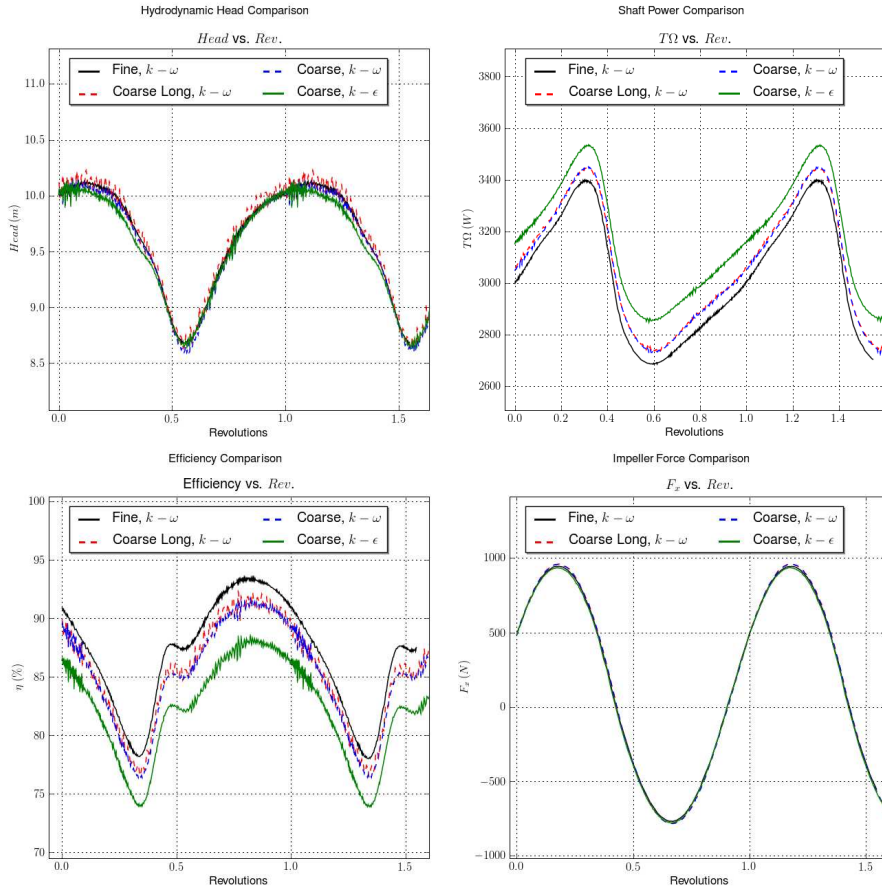


Figure 5: Comparison of computational performance behaviors:  $Head$  (top left),  $T\Omega$  (top right),  $\eta$  (bottom left) and  $F_x$  (bottom right).

The differences in modeling choices are most notable in the shaft power and efficiency

Grid, Turbulence Model	Total Head $H_{avg}$ (m)	Shaft Power $T\Omega_{avg}$ (W)	Efficiency $\eta_{avg}$ (%)
Fine, $k - \omega$ SST	9.60	2985	87.8
Coarse, $k - \omega$ SST	9.57	3037	85.9
Coarse Long, $k - \omega$ SST	9.62	3041	86.3
Coarse, $k - \varepsilon$	9.55	3137	83.0
Experiment	9.2	3250	78.0

Table 3: Comparison of computational, time-averaged (1 rev.) performance results. Experimental values are included for reference.

results. The standard  $k - \varepsilon$  model, by virtue of its more diffuse nature, predicts 7% higher viscous torque on the impeller than the **Coarse**  $k - \omega$  SST.

On the other hand, all the  $k - \omega$  SST simulations show surprisingly good mutual agreement regardless of the marked difference in grid resolutions. This evidently manifests the positive influence of having a high grid quality on a comparatively coarse mesh.

A comparison of the **Coarse** and **Coarse Long** results leads to a welcomed conclusion concerning the inlet boundary condition treatment: The influence of having a developed pipe flow profile at the inlet, instead of fixed values for  $\mathbf{U}$ ,  $k$ ,  $\omega$  and  $\varepsilon$ , is insignificant for performance analysis. Thus, the usage of the conventional model is well justified for design purposes.

The flow simulations demonstrated a relatively strict temporal accuracy requirement and a significant sensitivity to increasing the time step length. The effect of temporal accuracy can readily outweigh the effect of grid resolution or boundary condition treatment. For instance, increasing the time step to correspond to  $\Delta\theta = |\Omega| \Delta t = 1^\circ$ , the **Coarse**  $k - \omega$  SST performance results change as follow:  $H_{avg} = 9.45\text{m}$  (1.3%),  $T\Omega_{avg} = 3080\text{W}$  (1.4%),  $\eta_{avg} = 83.6\%$  ( $\Delta\eta = 2.3\%$ ), where the percentage difference is shown in parenthesis. Thus, if comparative studies between slightly changed geometries are conducted, it is important to employ the same computational settings and time steps. Otherwise the changes due to design alterations may be blurred by the differences in the numerical treatment. Since the numerical behavior of the pressure solution also changes with an increasing time step, Figure 6 is added to exemplify this phenomenon.

The juxtaposition of computational and experimental performance measures in Table 3 does not provide an apparently meaningful comparison since the complexity of the computational models has been reduced by neglecting specific details (see section 2.2) which complicate the CFD analysis. These neglected wet areas and leakages increase the

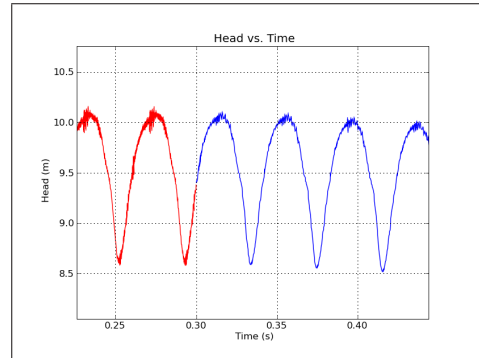


Figure 6: Illustration of the changes in solution behavior as  $\Delta t$  is increased. The change occurs at  $t = 0.30$ .

shaft power requirement and have a moderate adverse effect on the hydrodynamic head, which accounts for the fact that the CFD analysis ends up consistently over-predicting the performance. Since the effects of these extra loss mechanisms remain both predictable and uniform for a particular pump configuration, the utility of the experimental measurements remains essential.

### 3.2 Flow Behavior and Velocity Profile Comparison

While the performance data is crucial in evaluating the quality of the design, it does not provide any insight into the flow behavior of the system. In order to improve the design rules utilized in generating new pump geometries, the dependencies between characteristic flow phenomena and geometric attributes must be properly identified and understood, which, in turn, requires access to detailed information about the flow system. Experimental means offer a crucial, yet limited and expensive, contribution in the development, but when combined with high accuracy CFD analysis, the capacity to extract meaningful information on flow system dependencies increases dramatically. Therefore, as the utility of CFD analysis has been well established for performance predictions, greater emphasis has now been placed on gaining a more detailed description of the flow structures developing within the pump. This naturally requires a higher grid resolution, an appropriate turbulence model and a set of discretization schemes that do not suffer from considerable numerical diffusion. Despite these computationally demanding requirements, the scope of this analysis is deliberately limited to such URANS simulations that remain both computationally and practically feasible.

The **Fine** case has been prepared with the objective that, while the size of the computational grid remains moderate by current standards, the resolution of the simulated flow behavior is considerably increased compared to the **Coarse** model. In order to gain greater confidence in the transient CFD results produced by OpenFOAM, a set of time-accurate LDV velocity profile measurements were prepared for this study. Two sets of radial and tangential profiles, labeled *A* and *B*, were taken at two locations in the pump’s volute, shown in Figure 7, such that the second set of measurements were taken at a slightly different radial locations.

A tick marker fixed to the trailing edge of the blade was used to set  $\theta = 0$  where the trailing edge aligns with *W1*.

The animated velocity profile comparisons bring forth a captivating demonstration of the time-dependent behavior of the flow system and reveal the striking agreement on the fluctuating nature of the tangential and radial velocity fields, which unfortunately cannot be properly conveyed in this report. Although Figures 8 and 9 can only provide a glimpse

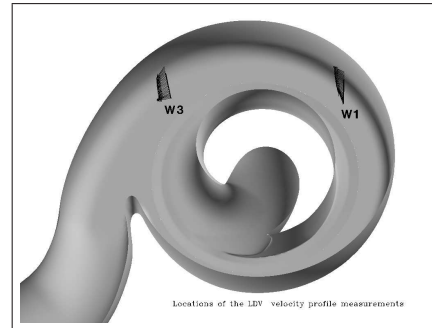


Figure 7: Time-accurate LDV velocity profile measurements were taken at the shown locations, *W1* and *W3*, for comparison.

of the time-accurate comparisons, they warrant support for the following deductions:

- All the models succeed in predicting the tangential velocity behavior with good accuracy.
- The measured radial profiles indicate that the pump generates a large swirling structure in the volute such that the flow bordering  $Z_{max}$  is outward while at  $Z_{min}$  it is inward. This undesired flow behavior is correctly captured by CFD.
- In the radial velocity profiles, particularly at  $W1$  shown in Figure 8, there is a consistent discrepancy within the range  $Z = 0.01 \rightarrow 0.03$  throughout the revolution of the impeller. It is suspected that this is due to leakage between the impeller and the volute, which is not included in the computational model.
- The differences between the **Coarse** and **Coarse Long** results are insignificant. The special treatment of the inlet boundary condition does not pay off in this respect either.
- Results generated by the **Fine** model demonstrate greater detail in the secondary flow structures, which are evident from the shape and behavior of the radial profiles.
- Although the **Coarse**  $k-\varepsilon$  solution captures the main flow characteristics, compared to the **Coarse**  $k-\omega$  SST cases, the results exhibit notably higher numerical damping.

As the animated time-accurate velocity profile comparisons are adjoined with a broader visualization of the flow field, as shown in Figure 10, a remarkably descriptive illustration of the flow behavior can be achieved. This is particularly striking with the **Fine** simulation, which lays out the evolution of a wide range of flow structures distinctly. Therefore, with the aid of well-prepared transient visualizations, different aspects of the oscillating flow system can be closely analyzed. For instance, the complex impeller-volute interaction of the pump emerged with an arresting resolution from the **Fine** analysis. Through proper visualizations, detailed information about this potentially detrimental transient phenomenon could be extracted. The strong interaction between the impeller and volute is exemplified in Figure 11.

In conclusion, the presented work, which applies an open-source CFD tool to a complex flow problem, leads to a tangible ramification: The study demonstrates the means to meet the ever-growing demand to conduct high-accuracy transient turbomachinery analysis routinely as a part of the design practice. As a corollary, even further cost efficiency can be obtained in design as increasingly detailed numerical testing ultimately reduces the need to construct expensive prototypes.

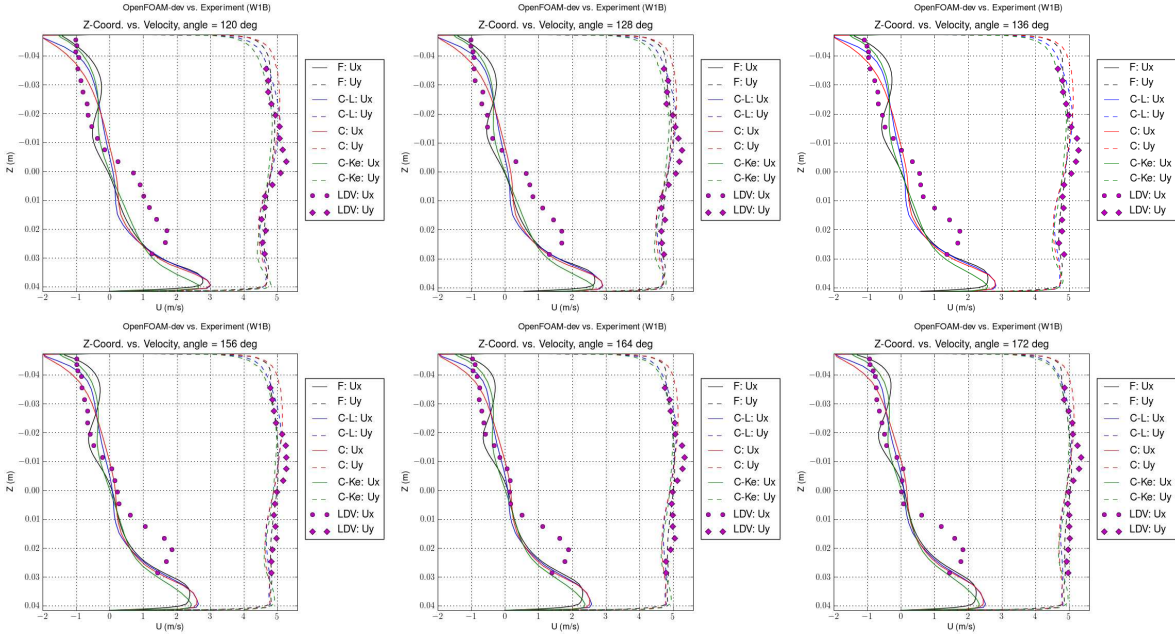


Figure 8: Snapshots from an animation depicting a time-accurate comparison of the radial ( $U_x$ ) and tangential ( $U_y$ ) velocity profiles obtained at measurement point W1. Abbreviations: F=Fine  $k - \omega$ , C-L=Coarse Long  $k - \omega$ , C=Coarse  $k - \omega$ , C-Ke=Coarse  $k - \varepsilon$

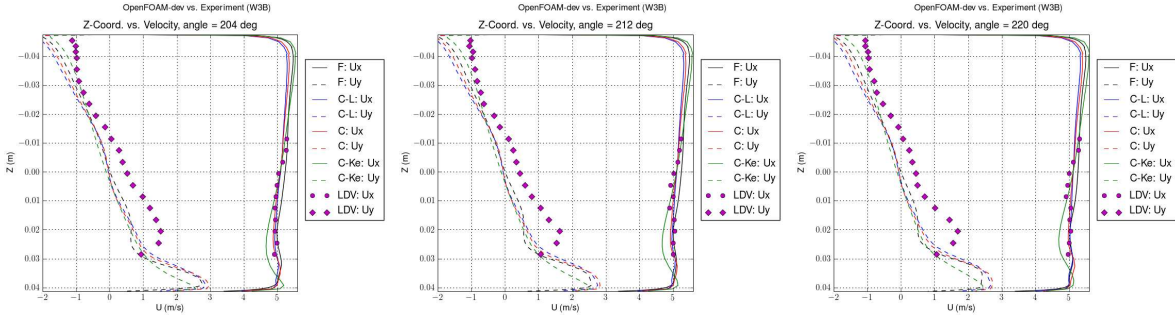


Figure 9: Snapshots from an animation depicting a time-accurate comparison of the radial ( $U_y$ ) and tangential ( $U_x$ ) velocity profiles obtained at measurement point W3.

## 4 CONCLUSIONS

- With the newly added utility of the GGI, detailed transient analysis of turbomachinery applications has become feasible with OpenFOAM.
- A transient solver which implements the SIMPLE pressure correction algorithm is shown to facilitate an efficient and robust transient analysis due to the ability to utilize a wide range of time step lengths. This is essential in the single-channel pump analysis because the flow solution goes through a lengthy development period before settling into

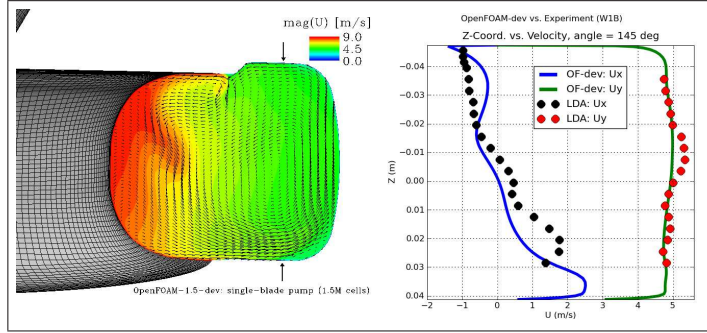


Figure 10: A combined illustration of the flow field across the  $y$ -plane. The location of the line along which W1 measurements were taken is marked by arrows.

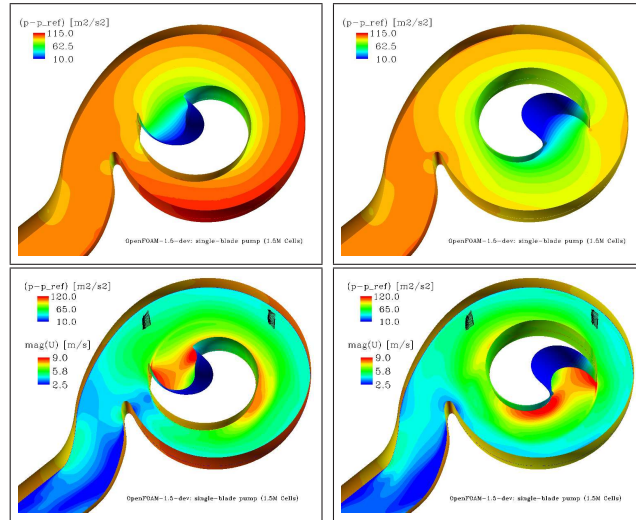


Figure 11: Visualizations of the pressure (top) and velocity (bottom) fields at different impeller angles.

a recurring periodic pattern.

- With high quality computational meshes, grid resolution does not influence the performance predictions notably. However, in order to resolve the characteristic flow structures of the pump, grid resolution becomes critical.
- The analysis indicates that it is sufficient to impose fixed value boundary conditions for velocity and turbulence variables at the inlet of the pump.
- The pressure solution remains practically unaltered as different turbulence models ( $k - \omega$  SST vs.  $k - \varepsilon$ ) are applied. On the other hand, clear differences manifest in the shaft power requirement values ( $T\Omega$ ) and in time-accurate velocity profile comparisons. The standard  $k - \varepsilon$  results clearly suffer from excessive diffusion.
- As the time step is reduced and the mean Courant number  $CFL$  of the computation

becomes sufficiently small, the pressure field begins to demonstrate small fluctuations. However, this numerical behavior does not have a notable effect on the performance or the velocity field behavior.

- The time-accurate LDV velocity profile comparisons together with detailed visualizations attest that the high grid resolution model succeeds in resolving the flow system with striking detail. Although some details of the pump configuration have been omitted in the CFD model, the complex fluctuating behavior of the flow can be successfully captured.

## REFERENCES

- [1] M. Auvinen, J. Ala-Juusela, L. Ilves, T. Siikonen, Dissecting a Complex System; A Computational Study of Flow Behavior in a Single-Blade Pump, *5th International Conference on Heat Transfer, Fluid Mechanics and Thermodynamics, HEFAT 2007*, Sun City, South Africa, July 1-4, (2007)
- [2] H.G. Weller, G. Tabor, H. Jasak, and C. Fureby, A Tensorial Approach to Computational Continuum Mechanics Using Object Orientated Techniques, *Computers in Physics*, **12**(6), pp. 620 - 631, (1998)
- [3] M. Beaudoin, H. Jasak, Development of a Generalized Grid Interface for Turbomachinery simulations with OpenFOAM, *Open Source CFD International Conference 2008*, Berlin, Germany, December 4-5, (2008)
- [4] P. Petit, M. Page, M. Beaudoin, H. Nilsson, The ERCOFTAC centrifugal pump OpenFOAM case-study, *3rd IAHR International Meeting of the Workgroup on Cavitation and Dynamic Problems in Hydraulic Machinery and Systems*, October 14-16, Brno, Czech Republic, (2009)
- [5] P.D. Thomas, C.K. Lombard, Geometric Conservation Law and Its Application to Flow Computations on Moving Grids, *AIAA Journal*, **17**, pp. 1030-1037, (1979)
- [6] H. Jasak and Z. Tukovic, Automatic Mesh Motion for the Unstructured Finite Volume Method, *Transactions of FAMENA*, **30**(2), pp. 1-18, (2007)
- [7] R.I. Issa, Solution of the Implicitly Discretised Fluid Flow Equations by Operator-Splitting, *Journal of Computational Physics*, **62**(11), pp. 40-65, (1986)
- [8] S.V. Patankar, Numerical Heat Transfer and Fluid Flow, *Hemisphere Publishing Corporation* (1980)
- [9] H. Jasak, Error Analysis and Estimation for Finite Volume Method with Applications to Fluid Flows, Ph.D. Thesis, Imperial College, University of London, (1996)

- [10] GridPro, Program Development Company, White Plains, NY 10601, USA  
([www.gridpro.com](http://www.gridpro.com))
- [11] H. Jasak, H. G. Weller, A. D. Gosman, High Resolution NVD Differencing Scheme for Arbitrarily Unstructured Meshes, *Int. J. Numer. Meth. Fluids*, **31**, pp. 431-449, (1999)